Research Article | Vol. 11, No. 3 / 1 March 2020 / Biomedical Optics Express 1316
Biomedical Optics EXPRESS

Fiber optic interferometric immunosensor based on polydimethilsiloxane (PDMS) and bioactive lipids

MILDRED S. CANO-VELÁZQUEZ,[1,*] LUZ M. LÓPEZ-MARÍN,[2] AND JUAN HERNÁNDEZ-CORDERO[1]

[1] *Instituto de Investigaciones en Materiales, Universidad Nacional Autónoma de México, Ciudad Universitaria, 04510, Ciudad de México, Mexico*
[2] *Centro de Física Aplicada y Tecnología Avanzada, Universidad Nacional Autónoma de México, Boulevard Juriquilla 3001, Santiago de Querétaro, 76230, Querétaro, Mexico*
[*] *mildred.cano.vel@gmail.com*

Abstract: We demonstrate a novel and simple means to fabricate optical fiber immunosensors based on Fabry-Perot (F-P) interferometers using polydimethylsiloxane (PDMS) as support for bioactive lipids. The sensors are fabricated following a straightforward dip-coating method producing PDMS end-capped devices. A biosensing platform is realized by subsequent functionalization of the PDMS cap with a previously characterized bioactive lipid antigen cocktail from *Mycobacterium fortuitum*, used as a surrogate source of antigens for tuberculosis diagnosis. After functionalization of the PDMS, the F-P sensors were immersed in different antibody-containing sera and the registered changes in their spectral features were associated to the interactions between the active lipids and the serum antibodies. Our results show that the proposed PDMS end-capped F-P immunosensors perform well differentiating antibody-containing sera. Furthermore, they offer attractive attributes such as label-free operation, real-time detection capabilities and they are also reusable. The proposed sensors, therefore, serve as an enabling optical immunosensing technique offering excellent potential for developing novel lipidomic analytical tools.

1. Introduction

Fiber-optic Fabry-Pérot interferometers (FFPIs) have been used extensively for measuring chemical and physical parameters. Strain, molar concentration, temperature and refractive index, to name a few, have been successfully monitored using fiber-based devices [1]. Amid the different techniques for fabricating extrinsic Fabry-Perot (FP) cavities, the use of polymer overlays on the tip of standard single-mode optical fibers has gained a lot of attention [2–7]. This is mostly due to the ease of processing of polymeric materials, which can be deposited following straightforward dip-coating procedures, and can be readily cured on the tip of the fibers. Several polymers have been shown to provide a suitable platform for developing the so-called polymer end-caps forming the F-P cavity in these structures. Refractive index, temperature, pressure, humidity and concentration measurements have been carried out with such configurations [2–6,8], yielding robust structures and in some cases with multi-variable sensing capabilities (e.g., pressure and temperature) [7]. For biosensing applications, adequate biocompatible platforms capable to support bioactive molecules for biorecognition are always required. Polymer platforms are commonly used for these purposes, and they typically require further treatment to promote its functionalization with these bioactive entities [9–11].

Among the available polymers, Polydimethylsiloxane (PDMS) has become one of the main choices for biomedical related applications owing to its biocompatibility, chemical inertness, haemocompatibility, and optical transparency [12–15]. It is further easy to process, flexible and has low surface energy allowing for creating complex arrays for microfluidic biosensors

#379518 https://doi.org/10.1364/BOE.379518
Journal © 2020 Received 1 Oct 2019; revised 29 Jan 2020; accepted 4 Feb 2020; published 10 Feb 2020

Biomedical Optics EXPRESS

and for miniaturizable detection systems [16–18]. However, the high hydrophobicity of PDMS [19] has been considered as a disadvantageous feature for biosensing applications because these are mostly performed on aqueous-based systems. Biosensors generally rely on mediators of biological activity, including enzymes and other proteins, nucleic acids or peptides; consequently, several methods have been envisioned for surface modification of PDMS in order to promote the attachment of these hydrophilic molecules [15,20–23]. In contrast, the use of this versatile polymer for the attachment of molecular entities with total or partial hydrophobicity, such as lipidic molecules, has not yet been explored. In this paper, we demonstrate the use of PDMS functionalized with bioactive lipids as a suitable material for the development of a end-capped FFPI immunosensor.

The functionalization of the PDMS with bioactive lipids was performed by physisortion, via drop-casting, based on the hydrophobic nature of both, the polymer and the lipid [24]. To evaluate the performance of the proposed immunosensor, we used a lipid antigen cocktail from *Mycobacterium fortuitum* and the antibodies capable to recognize these lipid antigens. Such bacterial species have been previously used as a surrogate source of antigens for tuberculosis diagnosis [25,26]. The reactivity and differentiation capabilities of antibody-containing sera of the lipid-functionalized PDMS immunosensor was evaluated through spectral analysis. In particular, changes in the surrounding refractive index and dimensions of the end-cap, associated to the interactions between the active lipids and the serum antibodies, were effectively monitored by analyzing the spectral features of the FFPI. Our results demonstrate that the immunosensor is indeed able to recognize the sera antibodies offering an appropriate means for sera differentiation. We thus demonstrate an attractive lipidic platform for developing label-free immunosensors with real-time and direct detection capabilities.

2. Material and methods

2.1. Materials and biological samples

A Sylgard 184 silicone elastomer (PDMS) kit was purchased from Dow Corning, USA. Phosphate buffer saline (PBS) 1M was prepared by adding 80 g of NaCl, 2 g of KCl, 14.4 g of Na2HPO4 and 2.4 g of KH2PO4 to 800 mL of deionized water, adjusting to pH=7.4 and diluted to the 1 L mark of a test tube. 3% solution of BSA (purchased from Sigma Aldrich, USA) in PBS was used as blocking buffer. A denaturing potassium biphthalate buffer was used to detach antibodies from the antigen-functionalized PDMS. This buffering solution was prepared by mixing 100 ml 0.1 M potassium hydrogen phthalate and 44.6 ml of 0.1 M HCl, followed by pH adjustment to 3.0.

The bacterial lipid antigens for PDMS functionalization were extracted from *Mycobacterium fortuitum*, comprising a mixture of glycolipids of high antigenicity [27,28]. The lipid antigens were purified by adsorption chromatography in an open Florisil column eluted with chloroform, acetone, and methanol (3 volumes each), followed by a solid phase extraction of the acetonic fraction onto a silica gel Sep-Pak column (Waters, USA) washed with chloroform and eluted with freshly distilled acetone. The purified lipids were dried under nitrogen and kept at −20°C until use. To obtain specific hydrosoluble ligands against the purified lipid antigens, serum antibodies were raised in two white New-Zealand rabbits (2 months old). Briefly, the antigen-containing acetonic fraction was suspended in NaCl 0.85% (10 mg in 1.0 ml) and mixed with 1.0 ml of complete Freund adjuvant (Sigma Aldrich, USA). Each individual received a subcutaneous administration of 1.0 ml antigen cocktail. At 15 and 30 days post-immunization, each animal received boosts consisting of 3 mg antigen mixture in 0.5 ml 0.85% NaCl and 0.5 ml incomplete Freund adjuvant (Sigma Aldrich, USA). The subjects were bled before immunization to obtain Pre-immune, control serum (*PS*) (serum devoid of anti-lipid antibodies). A terminal bleed was performed at day 45 post-immunization to obtain a Hyper-immune serum (*HS*) (serum with high content of anti-lipid antibodies).

Biomedical Optics EXPRESS

2.2. Sensor fabrication and sensing principle

In order to fabricate a PDMS end-capped FFPI sensor [29], we used a simple dip-coating technique. A mixture of PDMS precursor and cross-linker (10:1 by mass) was prepared, mixed, degassed and pre-cured at 70°C during 15 min. This pre-curing process is essential to increase the viscosity of the PDMS drop in order to avoid Marangoni effects, which usually displace the polymer upwards along the fiber [30]. The polymer end-cap was realized by dipping the cleaved end face of a standard single-mode fiber (SMF-28e, Corning, USA) into a pre-cured drop of PDMS. A computer-controlled system for fiber positioning and pulling was used to set the appropriate velocities for driving the cleaved end-face of the fiber in and out of the pre-cured PDMS. Based on previous experiments for liquids analysis on optical fiber tips [30], the fiber displacement velocity was set to $1.7mm/s$ yielding a semi-spherical cap on the end face of the optical fiber. Afterwards, the end-capped sensor was vertically placed in an oven at 180 °C during 1 hour to fully solidify the PDMS. An image of the resulting fiber device is shown in Fig. 1(a).

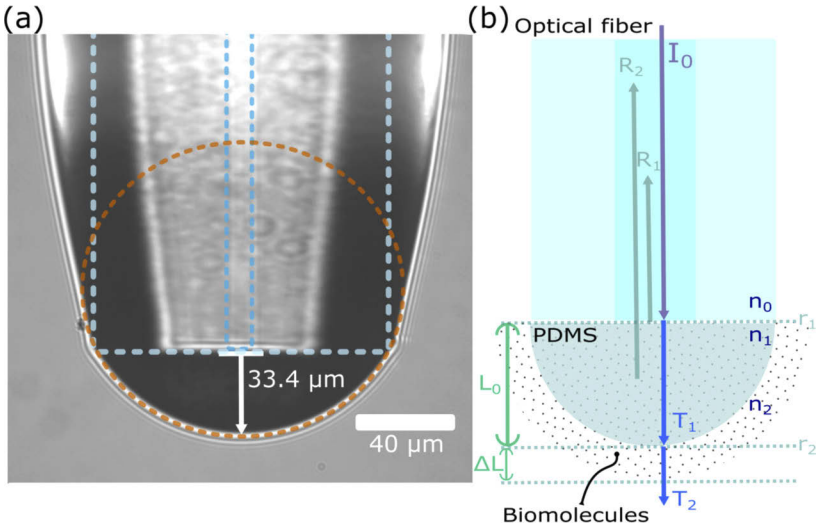

Fig. 1. Image (a) and schematic representation (b) of the fabricated fiber optic sensor. The end-cap at the tip of the fiber forms a Fabry-Pérot interferometer. The dashed blue lines depict the core and the cladding of the optical fiber.

As shown schematically in Fig. 1(b),the PDMS end-cap and the cleaved end-face of the fiber form a FFPI. The spectral response of the FFPI can be described using two beam interference theory considering the Fresnel reflections from the two interfaces: the end-face of the fiber (core refractive index n_0) and the surface of the PDMS end-cap (reflection coefficients r_1 and r_2, respectively). Both interfaces are separated by the PDMS cap, with length L_0 and refractive index n_1. With this arrangement, the total reflected intensity from the FFPI (I_R) is given by [9,30]:

$$I_R = \frac{r_1^2 + 2r_1 r_2 \cos(\phi) + r_2^2}{1 + 2r_1 r_2 \cos(\phi) + r_1^2 r_2^2} \tag{1}$$

where $r_1 = \frac{n_1 - n_0}{n_0 + n_1}$, $r_2 = \frac{n_2 - n_1}{n_1 + n_2}$, and the phase difference is:

$$\phi = \frac{4\pi n_1 L_0}{\lambda} \tag{2}$$

where λ is the wavelength of the incident light.

Biomedical Optics EXPRESS

According to Eqs. (1) and 2, the intensity pattern I_R is affected by variations of the refractive indices of the PDMS (n_1) and the surrounding medium (n_2), as well as by changes in the length of the resonant cavity (L_0). Therefore, when the bio-molecules are attached to the sensor surface, the interference pattern will shift in wavelength ($\Delta\lambda$) owing to changes in the effective length (ΔL) and in the surrounding refractive index (Δn_2) [9,30]. The spectral shift can thus be associated with the modification of the PDMS surface due to the antigen attachment and further interactions of the sensor tip with the antibodies during the immunosensing test.

2.3. Characterization of the lipid-ligand system

For our experiments, a mixture of well-known lipid antigens was purified from *M. fortuitum* and used to produce anti-lipid antibodies in rabbits. The obtained antigen-antibody pair was then used to explore whether PDMS was suitable to immobilize a bioactive lipid (i.e. the mycobacterial cocktail antigen) and for promoting the capture of antibodies. Common protocols for lipid immobilization rely on the attachment of a very little amount of the lipid substance on the material surface; hence, a highly sensitive method is frequently necessary to assess the binding. Given the antigen nature of the lipids used in this report, an immune assay (i.e. indirect ELISA protocol [31]) with Pre-immune serum (*PS*) and Hyper-immune serum (*HS*) was performed on PDMS to evaluate the antigen-antibodies interaction.

Briefly, for the indirect ELISA protocol, the PDMS surface was coated by drop-casting with the lipid antigen diluted in ethanol-hexane (1:1, v/v); then the reactivity of the lipids to specific antibodies was measured with a secondary antibody linked to alkaline phosphatase, an enzyme for the development of color as a final signal. In this kind of assay, the values of the optical density (OD) are directly associated with the degree of antigen-antibody binding [31]. Different doses of rabbit sera were used to explore the ability of the functionalized PDMS to capture anti-lipid antibodies. Each serum was prepared in 0.3% BSA in PBS, using a log_2 serial dilution (1:100, 1:200, 1:400, 1:800, 1:1600, 1:3200, 1:6400, 1:12800), for a fixed unbiased antigen concentration of $64(\mu g/100\mu L)$. Similarly, to optimize the antigen concentration yielding the highest immunoreaction, the PDMS was functionalized by deposition of log_2 serial concentrations of lipid antigen onto the PDMS-containing wells, keeping fixed the optimum serum dilution obtained from the previous set of experiments. Hence, $300\mu L$ of the antigen were deposited at concentrations of 64, 32, 16, 8, 4, 2, 1, 0 ($\mu g/100\mu L$). All experiments were performed in triplicates.

The ELISA results for both set of experiments are shown in Fig. 2. As seen in the figure, mycobacterial lipid antigens readily allowed the capture of rabbit specific antibodies. In all cases, the reactivity of Hyper-immune serum (*HS*), rich in specific anti-lipid antibodies, was found to be larger than that of the control serum (*PS*). These data show that the lipid antigen maintain their bioactivity after attachment on the PDMS, thereby demonstrating the suitability of this polymer for immobilization of these molecules. From these plots we further obtain that a maximum capture of serum antibodies is achieved for a serum dilution of 1 : 400 (Fig. 2(a)) and an antigen concentration of $8(\mu g/100\mu L)$ (Fig. 2(b)).

2.4. Functionalization of the FFPI sensor and direct immunoassay

Figure 3 shows the steps followed to functionalize and test the performance of the FFPI immunosensor. For PDMS functionalization, mycobacterial lipid antigens were immobilized on the end-capped sensor. This was achieved upon immersing the device in $0.5mL$ of ethanol-hexane (1:1, v/v) with an antigen concentration of $8(\mu g/100\mu L)$ for 30 minutes, followed by a 15 minutes drying process at room temperature (step 1). Free binding sites were blocked by immersing the sensor tip in $200\mu L$ of 3% BSA for 30 min at 37 °C (step 2), followed by three consecutive immersion washes in PBS ($300\mu L$) (step 3). A total of three sensors were functionalized and treated following this procedure.

Biomedical Optics EXPRESS

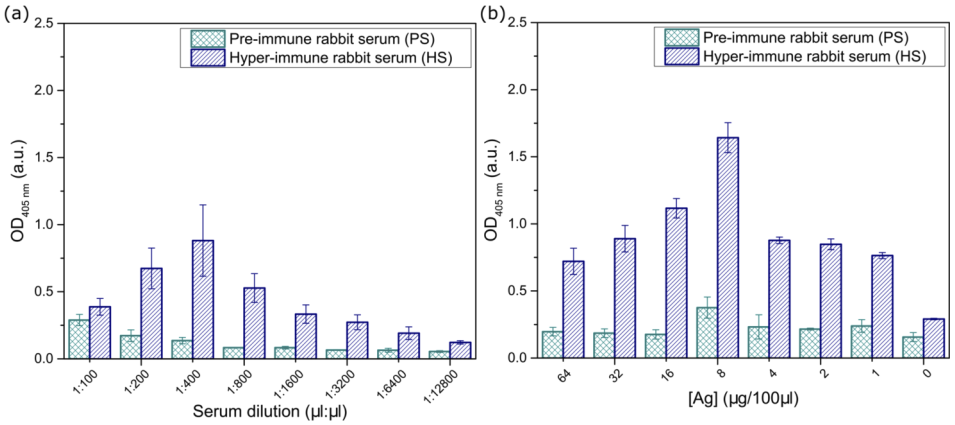

Fig. 2. ELISA results for antibody capture by the mycobacterial lipid antigen deposited onto PDMS. Results are shown for control, Pre-immune (*PS*) and specific antibody-containing Hyper-immune (*HS*) sera from lipid-immunized rabbits. (a) Results for $64(\mu g/100\mu L)$ of mycobacterial lipid antigens deposited onto PDMS at 2-fold serial dilution of sera ($1:100$ to $1:12800(\mu L/\mu L)$). (b) Results for lipid antigens deposited at increased concentrations ($0\text{-}64(\mu g/100\mu L)$), keeping a serum dilution of $1:400(\mu L/\mu L)$. Each bar represents the mean OD ± the standard errors from triplicate measurements.

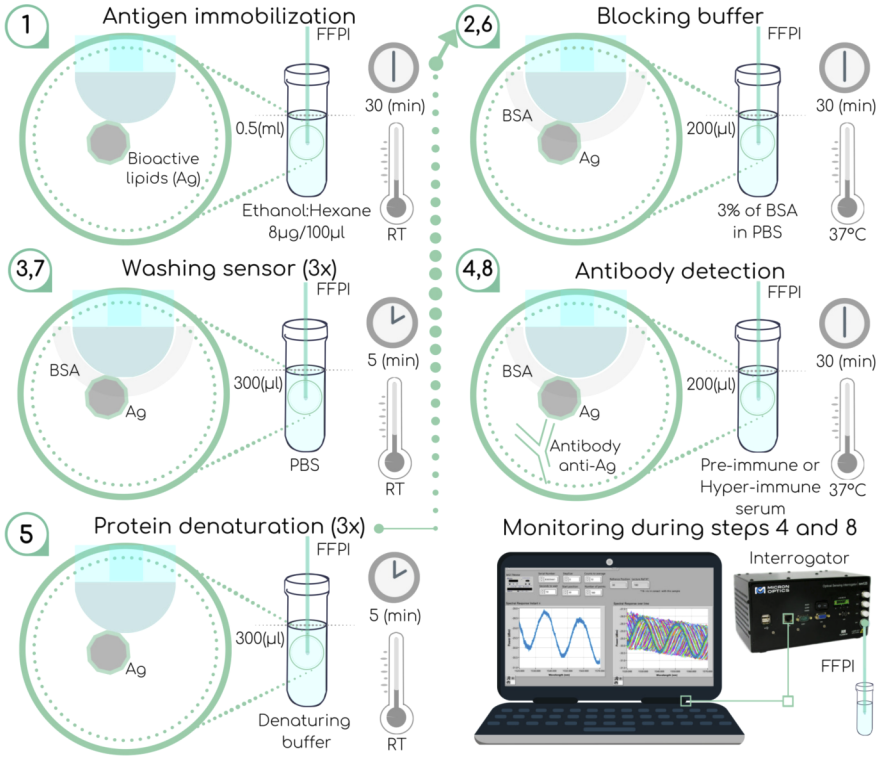

Fig. 3. Procedure for functionalization of the FFPI sensor and for direct immunoassay tests (see text for details).

Biomedical Optics EXPRESS

Antibody binding on the functionalized PDMS end-cap was explored by immersing the devices in Pre-immune (*PS*) and Hyper-immune (*HS*) sera. Each sensor was first immersed in $200\mu L$ of pre-immune serum dilution ($1:400(\mu L/\mu L)$cuando) during 30 min at 37 °C (step 4). Subsequently, the same sensors were used for testing hyper-immune serum after removing the bound lipid ligands attached to the PDMS cap. This was done by immersion (3 times) in a denaturalizing buffer solution with pH 3 (step 5). The free binding sites on the fiber tips were immersed again in BSA for blocking (step 6) and finally washed three consecutive times in PBS ($300\mu L$) (step 7). Following this process, the tips were immersed in $200\mu L$ of $1:400(\mu L/\mu L)$ hyper-immune serum dilution during 30 min at 37 °C (step 8).

While immersed in the *PS* and *HS* sera, the back-reflected interferometric signal at $1550nm$ from the sensors was continuously monitored using a fiber Bragg grating interrogator (Micron Optics, sm125) and a virtual instrument for automatic acquisition of the spectra. The spectral response (i.e. interference pattern) of the immunosensor was acquired every $10s$ during $30min$. After these measurements were performed, the shift in wavelength ($\Delta\lambda$) over time was obtained by cross-correlation of the acquired spectra. This was done using the built-in Matlab algorithm and cross-correlating the reference signal (interference pattern acquired at $t = 0$) with the patterns acquired over time. The cross-correlation yields a maximum value indicating the corresponding wavelength shift, hence, the temporal evolution of $\Delta\lambda$ can be readily obtained.

Because the sera are kept under incubation conditions (37 °C), thermal effects are expected to contribute to the shift in wavelength registered by the sensors. This is mainly due to the thermal expansion coefficient of the PDMS (3.2 x $10^{-4\circ}C^{-1}$), that will lead to a change in the effective length (ΔL) of the FP cavity. To account for this contribution, separate experiments were performed for registering the change in wavelength ($\Delta\lambda$) while the immunosensor was immersed in PBS at 37 °C during 30 minutes. Similarly, in order to verify that the trends in $\Delta\lambda$ obtained when testing *PS* and *HS* sera are only due to antigen-antibody interactions, untreated sensors (i.e., without the lipid antigen) were immersed in both sera. Under this conditions, no immuno-reaction should be expected and $\Delta\lambda$ should be the same for both sera.

3. Results and discussion

3.1. Sensors features

As part of the characterization of the fabricated FFPI sensors, the spectral response of the device was monitored continuously during the different stages of the fabrication process. Spectra was thus acquired before PDMS deposition and until the curing of the PDMS end-cap was finished; images of the probe were acquired during the dip coating and after the curing process with an InfinyTube system coupled with a 10x microscope objective, keeping the same focal plane. Figure 4 shows the spectral response and images for these different stages. First, during the immersion of the tip on PDMS *(case (a))*, there is no interferometric signal since a cavity is not defined at this stage. Once the fiber is pulled out from the PDMS, the end-cap is formed and an interference pattern is clearly visible *(case (b))*. When the curing process starts, the Extinction Ratio of the interferometric signal ($ER = P_{max} - P_{min}$) increases as a result of the higher refractive index within the cavity due to the thermal curing process [29]. While kept at a constant temperature (180°C) for curing, the interference pattern experiences a blue-shift associated to a decrease in cavity length. This is noticeable in the spectra shown in *(c)* and *(e)* and is also apparent upon comparing the corresponding images. Finally, a comparison between the interference patterns displayed in *(d)* and *(e)*, shows that no significant changes are apparent in the spectra. Hence, after a total curing time of approximately 25 min the PDMS end-cap is completely cured and the physical dimensions and refractive index remain constant.

Since all the relevant parameters for the dipping process are kept under control (i.e., initial volume of PDMS and pre-curing conditions, fiber pulling velocities and final curing of the end-cap), the fabrication procedure consistently yields sensors with similar characteristics. For

Biomedical Optics EXPRESS

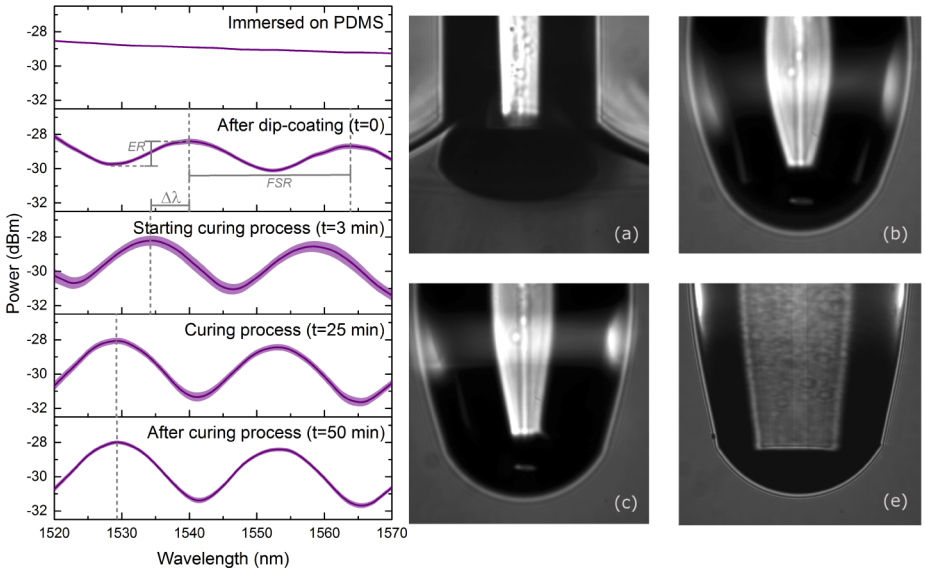

Fig. 4. Interference patterns obtained during the end-cap deposition on the tips of single-mode fibers. The shadows on the curves represent the standard deviation from three different fabricated sensors. The images show the fiber tip during immersion, after extraction from the PDMS, and at the initial and final moments of the curing process (see text for details).

all of the three sensors presented in this paper, the spectral features and their respective free spectral ranges FSR are similar ($24.88 \pm 0.02nm$), corresponding to an effective cavity length (cap size) of approximately $33.42 \pm 0.03\mu m$.

3.2. Antigen immobilization and immunoassay results

Typical spectra obtained from our experiments showing the time evolution of the interference pattern for different stages of the immunoassay are shown in Fig. 5(a). For all the stages shown in the figure, the interference patterns shift over time towards longer wavelengths (red shift) while the tip is immersed in the solutions. These shifts correspond to an increase in the optical thickness due to the attachment of the bio-layer onto the PDMS end-cap. This is evident even from the functionalization process: the spectral features of the interference pattern of the sensor experiences both, a wavelength shift ($\Delta\lambda = 4.28nm$), a change in extinction ratio ($\Delta ER = 0.53dBm$) and a change in free spectral range ($\Delta FSR = 0.1nm$), thereby confirming the antigen immobilization on the PDMS.

The shifts in wavelength over time ($\Delta\lambda$) obtained from cross-correlation of the acquired spectra for the different tested scenarios are plotted in Fig. 5(b). Notice first that thermal expansion effects are clearly visible from the sensor readout: after the sensor tip is immersed in PBS at 37 °C, $\Delta\lambda$ increases reaching a maximum after 30 minutes *(curve A)*. At this time, the PDMS cap seems to reach its maximum length due to thermal expansion. For the FFPI without lipid antigens *(curves B and C)*, a wavelength shift ($\Delta\lambda_i$) is initially registered upon immersion in the sera (either *PS* or *HS*) owing to the difference in refractive indices of these solutions and the PBS [32–34]. Once immersed in the *PS* and the *HS* solutions, $\Delta\lambda$ has a very similar trend to that obtained in PBS *(curve A)*. This trend in wavelength shift is thus attributed to thermal expansion effects leading to an increase in length of the PDMS cavities. We can thus conclude that there is no attachment of antibodies on the FFPI without the antigen; thus, neither the *PS* nor the *HS* can be identified properly. Furthermore, this confirms that immunosensing is not achieved

Biomedical Optics EXPRESS

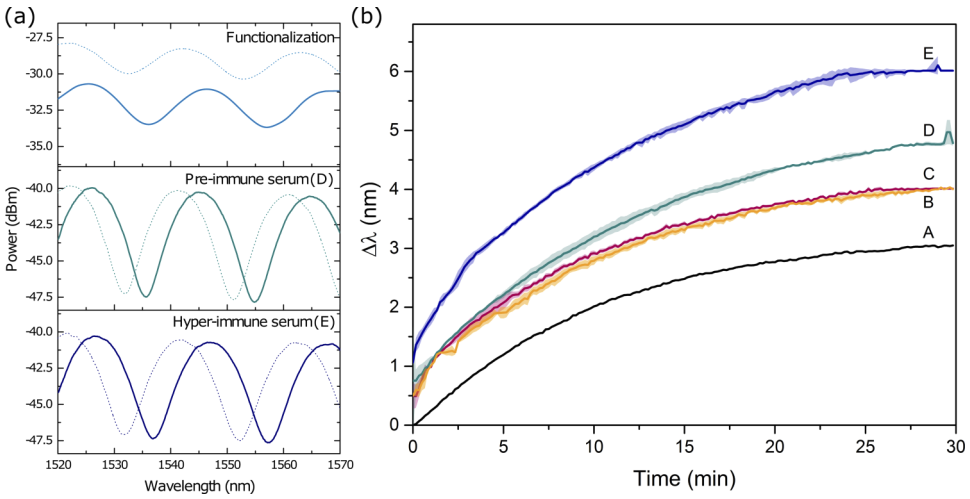

Fig. 5. (a) Spectral response of the fabricated end-capped sensor at different stages of the immunoassay: functionalization with antigenic lipids and immersion in Pre-immune and Hype-immune sera. The dashed and the continuous lines represent the first and last acquired interference pattern, respectively. (b) Wavelength shift ($\Delta\lambda$) during detection of antigen-antibody binding on PDMS. Curves A, B and C show the performance of untreated (i.e., without the lipid antigen) sensors during incubation in PBS (T=37 °C) (A), control (*PS*) (B) and specific antibody-containing Hyper-immune (*HS*) (C) sera from lipid-immunized rabbits ($1:400(\mu L/\mu L)$). Curves D and E were obtained with functionalized sensors immersed in *PS* (D) and *HS* (E) sera (see text for details). The shadows on the curves represent the standard deviation from triplicate measurements.

through polymer-antibodies interactions, and that as shown below, the antigen functionalization is therefore essential for antibody detection.

The wavelength shifts obtained with the functionalized sensors when immersed in both sera (*PS* and *HS*) are shown in curves *D* and *E* of Fig. 5(b). While $\Delta\lambda$ still changes over time showing the thermal expansion effects of PDMS, the maximum wavelength shifts obtained with both sera (*PS* and *HS*) are larger than those registered for the other devices (curves *D* and *E*). Furthermore, the trend of these curves is different to those obtained for curves *A*, *B* and *C*, which are driven mostly by thermal expansion effects. This suggests that antibody binding on the functionalized PDMS cap indeed has an effect on the spectral response of the sensors. Notice further that the $\Delta\lambda$ registered during immersion in the *HS* serum (curve *E*) is larger than that obtained with the *PS* serum (curve *D*) ($\Delta\lambda_{HS} = 4.95nm$ vs. $\Delta\lambda_{PS} = 4.03nm$). This is a reasonable outcome as the *HS* serum contains a larger number of specific antibodies, thus increasing the binding events and thereby leading to a larger $\Delta\lambda$. It is also important to remark that the readouts for the *HS* serum were collected after cleaning and blocking the probes once the results for *PS* were obtained. This therefore confirms that the antigen coating is preserved on the PDMS cap and the sensors can be readily reused after simple protein denaturation washes. Thus, the capabilities of the immunosensor based on PDMS functionalized with lipid ligands seem to scale well to suitable specific antibody detection and serum differentiation with attractive features (e.g. label-free and reusable system with real-time and direct detection, and facile fabrication and functionalization process). Table 1 shows a summary of our results. For comparative purposes, we can estimate the difference between the maximum wavelength shift ($\Delta\lambda_f$) and the initial shift registered during immersion of the devices ($\Delta\lambda_i$). This difference ($S_{\Delta\lambda} = \Delta\lambda_f - \Delta\lambda_i$) represents the effective shift in wavelength due to thermal effects and any antigen-antibody interactions. Clearly, the largest

Biomedical Optics EXPRESS

$S_{\Delta\lambda}$ is achieved for the Hyper-immune (*HS*) serum and further shows a marked difference with the Pre-immune (*PS*) ($0.92nm$). Thus, the FFPI immunosensor based on PDMS functionalized with bioactive lipids is able to properly differentiate between different antibody-containing sera.

Table 1. Wavelength shifts ($\Delta\lambda$) achieved for the different immunoassays during incubation

Curve	Antigen	Solution	$\Delta\lambda_i$	$\Delta\lambda_f$	$S_{\Delta\lambda}$
A	Yes	PBS	0	3.05	3.05
B	No	PS	0.49	4.01	3.52
C	No	HS	0.50	4.01	3.51
D	Yes	PS	0.75	4.78	4.03
E	Yes	HS	1.06	6.01	4.95

The wavelength shift occurring during the immunoassay test can be estimated as [9]:

$$\Delta\lambda = \frac{\lambda(n_1 + \Delta L)(L_0 + \Delta n)}{n_1 L_0} \tag{3}$$

Considering the constributions by the bio-layer and the thermal effects in the PDMS, the changes in length and refractive index (ΔL and Δn) can be expressed as:

$$\Delta L = L_{bio} + (\alpha_L \Delta T L_0) \tag{4}$$

$$\Delta n = n_{bio} + (\alpha_n \Delta T n_1) \tag{5}$$

where ΔT is the increase in temperature, $\alpha_L = 3.2x10^{-4}\frac{1}{^\circ C}$ and $\alpha_n = -1.8x10^{-4}\frac{1}{^\circ C}$ correspond to the thermal expansion and thermo optic coefficients of PDMS, respectively [35,36]. Using these values and our experimental conditions ($L_0 = 33.42\mu m$, $n_1 = 1.3997$ [37], $\Delta T = 37^\circ C - 23^\circ C = 14^\circ C$, and $\lambda = 1550nm$), Eq. (3) can be rewritten as:

$$\Delta\lambda = 3.04nm + (46.38x10^{-3})L_{bio} + (1.1x10^{-6})n_{bio} \tag{6}$$

The first term in this expression represents the thermal effects contributing to the shift in wavelength. Notice that this value agrees well with the $S_{\Delta\lambda}$ obtained for the untreated sensors (i.e., without the antigen, curves *A*, *B* and *C*). In these cases, there is no antigen-antibody interactions and only thermal effects are expected to produce a shift in wavelength. For the functionalized sensors (curves *D* and *E*), the wavelength shifts due to bio-recognition effects might be evaluated upon substracting the thermal effects contributions (i.e., $S_{\Delta\lambda} - 3.53nm$). This yields $0.50nm$ and $1.42nm$ for the Pre-immune (*PS*) and the Hyper-immune (*HS*) serum, respectively. According to Eq. (6) the contribution of the bio-layer thickness is much larger than its refractive index. Thus, neglecting the last term in this equation we can estimate that the bio-layer attached to the immunosensor for pre-immune serum has a thickness of $10.78nm$, while for hyper-immune serum reaches $30.61nm$. Note that these layers include the antigen coating and any antibodies that could have attached to the functionalized PDMS surface. Hence, considering that the tests were performed with the same immunosensors, the thickness difference could be attributed to changes in the PDMS end-cap surface owing to antigen-antibody binding effects, as resported previously for other bio-sensing platforms [9,38].

4. Conclusions

We have demonstrated the detection of antibodies with a fiber optic sensor based on PDMS and bioactive lipids. Our results show than the proposed FFPI immunosensor is able to differentiate antibody-containing sera through changes in the spectral features of the device. These are

Biomedical Optics EXPRESS

associated to the interactions between the active lipids and the serum antibodies. The FFPI immunosensor shows attractive features such as ease of fabrication, label-free operation, real-time monitoring capabilities and reusability. Because sensing is based on antigen-antibody interaction, the end-capped devices may be used for detection of any type of target molecule, provided a proper antigen is immobilized on the PDMS. To the best of our knowledge, this is the first report showing that PDMS holds good functionalization capabilities by simple deposition of lipid mediators. Evidently, further studies are needed to assess the usefulness of PDMS for the immobilization of other bioactive lipids. Nonetheless, our results demonstrate a novel means for fabrication of optical biosensors for lipidomics tools analysis, such as those needed for the screening of unknown ligands or their reactivity with human fluid components (biomarkers of diseases, for instance) which require the availability of supports for bioactive lipids attachment. Indeed, the exploration of PDMS functionalized with mycobacterial lipid antigens, such as the one presented here, is highly encouraging for the diagnosis tuberculosis, currently one of the top killer diseases worldwide.

Funding

Dirección General de Asuntos del Personal Académico, Universidad Nacional Autónoma de México (PAPIIT IG100519).

Disclosures

The authors declare that there are no conflicts of interest related to this article.

References

1. K. Menghrajani, "Fibre-optic Fabry–Perot sensors: an introduction," (2018).
2. X. Tan, Y. Geng, X. Li, Y. Deng, Z. Yin, and R. Gao, "UV-curable polymer microhemisphere-based fiber-optic Fabry–Perot interferometer for simultaneous measurement of refractive index and temperature," IEEE Photonics J. **6**(4), 1–8 (2014).
3. X.-Y. Zhang, Y.-S. Yu, C.-C. Zhu, C. Chen, R. Yang, Y. Xue, Q.-D. Chen, and H.-B. Sun, "Miniature end-capped fiber sensor for refractive index and temperature measurement," IEEE Photonics Technol. Lett. **26**(1), 7–10 (2014).
4. I. Hernández-Romano, M. A. Cruz-Garcia, C. Moreno-Hernández, D. Monzón-Hernández, E. O. López-Figueroa, O. E. Paredes-Gallardo, M. Torres-Cisneros, and J. Villatoro, "Optical fiber temperature sensor based on a microcavity with polymer overlay," Opt. Express **24**(5), 5654–5661 (2016).
5. O. Arrizabalaga, J. Velasco, J. Zubia, I. S. de Ocáriz, and J. Villatoro, "Miniature interferometric humidity sensor based on an off-center polymer cap onto optical fiber facet," Sens. Actuators, B **297**, 126700 (2019).
6. M. Li, Y. Liu, S. Qu, and Y. Li, "Fiber-optic sensor tip for measuring temperature and liquid refractive index," Opt. Eng. **53**(11), 116110 (2014).
7. A. Guermat, A. Guessoum, N.-E. Demagh, M. Zaboub, and Z. Bouhafs, "Fibre-optic temperature and pressure sensor based on a deformable concave micro-mirror," Sens. Actuators, A **270**, 205–213 (2018).
8. J.-F. Hu and C.-P. Yu, "Microlens-based fiber Fabry-Pérot interferometer for the measurement of the concentration of sugar solution," in *2014 OptoElectronics and Communication Conference and Australian Conference on Optical Fibre Technology*, (IEEE, 2014), pp. 821–822.
9. Y.-T. Tseng, Y.-J. Chuang, Y.-C. Wu, C.-S. Yang, M.-C. Wang, and F.-G. Tseng, "A gold-nanoparticle-enhanced immune sensor based on fiber optic interferometry," Nanotechnology **19**(34), 345501 (2008).
10. L. Chen, C. Chan, R. Menon, P. Balamurali, W. Wong, X. Ang, P. Hu, M. Shaillender, B. Neu, P. Zu, Z. Tou, C. Poh, and K. Leong, "Fabry–Perot fiber-optic immunosensor based on suspended layer-by-layer (chitosan/polystyrene sulfonate) membrane," Sens. Actuators, B **188**, 185–192 (2013).
11. R. B. Queirós, S. Silva, J. Noronha, O. Frazão, P. Jorge, G. Aguilar, P. Marques, and M. G. F. Sales, "Microcystin-lr detection in water by the Fabry–Pérot interferometer using an optical fibre coated with a sol–gel imprinted sensing membrane," Biosens. Bioelectron. **26**(9), 3932–3937 (2011).
12. K. F. Lei, "Microfluidic Systems for Diagnostic Applications: A Review," J. Lab. Autom. **17**(5), 330–347 (2012).
13. S. Agrawal, K. Paknikar, and D. Bodas, "Development of immunosensor using magnetic nanoparticles and circular microchannels in PDMS," Microelectron. Eng. **115**, 66–69 (2014).
14. J. N. Patel, B. L. Gray, B. Kaminska, and B. D. Gates, "Flexible glucose sensor utilizing multilayer pdms process," in *2008 30th Annual International Conference of the IEEE Engineering in Medicine and Biology Society*, (IEEE, 2008), pp. 5749–5752.

Biomedical Optics EXPRESS

15. F. Gaudiiere, I. Masson, S. Morin-Grognet, O. Thoumire, J.-P. Vannier, H. Atmani, G. Ladama, and B. Labat, "Mechano-chemical control of cell behaviour by elastomer templates coated with biomimetic Layer-by-Layer nanofilms," Soft Matter **8**(32), 8327–8337 (2012).
16. J. Friend and L. Yeo, "Fabrication of microfluidic devices using polydimethylsiloxane," Biomicrofluidics **4**(2), 026502 (2010).
17. K. Jiang, P. C. Thomas, S. P. Forry, D. L. DeVoe, and S. R. Raghavan, "Microfluidic synthesis of monodisperse PDMS microbeads as discrete oxygen sensors," Soft Matter **8**(4), 923–926 (2012).
18. C. Badre, J. P. Chapelab, and S. Yang, "Selective dry and reversible transfer-printing of nanoparticles on top of PDMS wrinkles," Soft Matter **7**(21), 9886–9889 (2011).
19. D. Bodas and C. Khan-Malek, "Hydrophilization and hydrophobic recovery of PDMS by oxygen plasma and chemical treatment-an sem investigation," Sens. Actuators, B **123**(1), 368–373 (2007).
20. E. Jastrzebska, A. Zuchowska, S. Flis, P. Sokolowska, M. Bulka, A. Dybko, and Z. Brzozka, "Biological characterization of the modified poly (dimethylsiloxane) surfaces based on cell attachment and toxicity assays," Biomicrofluidics **12**(4), 044105 (2018).
21. T. Goda, T. Konno, M. Takai, T. Moro, and K. Ishihara, "Biomimetic phosphorylcholine polymer grafting from polydimethylsiloxane surface using photo-induced polymerization," Biomaterials **27**(30), 5151–5160 (2006).
22. F. Tian, J. Lyu, J. Shi, F. Tan, and M. Yang, "A polymeric microfluidic device integrated with nanoporous alumina membranes for simultaneous detection of multiple foodborne pathogens," Sens. Actuators, B **225**, 312–318 (2016).
23. J.-H. Seo, T. Shibayama, M. Takai, and K. Ishihara, "Quick and simple modification of a poly (dimethylsiloxane) surface by optimized molecular design of the anti-biofouling phospholipid copolymer," Soft Matter **7**(6), 2968–2976 (2011).
24. D. L. Nelson, A. L. Lehninger, and M. M. Cox, *Lehninger Principles of Biochemistry* (Macmillan, 2008).
25. X. Tan, M. K. Khaing Oo, Y. Gong, Y. Li, H. Zhu, and X. Fan, "Glass capillary based microfluidic elisa for rapid diagnostics," Analyst **142**(13), 2378–2385 (2017).
26. F. Hou, Q. Zhang, J. Yang, X. Li, X. Yang, S. Wang, and Z. Cheng, "Development of a microplate reader compatible microfluidic chip for ELISA," Biomed. Microdevices **14**(4), 729–737 (2012).
27. L. Escamilla, R. Mancilla, W. Glender, and L.-M. López-Marín, "Mycobacterium fortuitum glycolipids for the serodiagnosis of pulmonary tuberculosis," Am. J. Respir. Crit. Care Med. **154**(6), 1864–1867 (1996).
28. L. M. López-Marín, E. Segura, C. Hermida-Escobedo, A. Lemassu, and M. C. Salinas-Carmona, "6, 6'-dimycoloyl trehalose from a rapidly growing mycobacterium: an alternative antigen for tuberculosis serodiagnosis," FEMS Immunol. Med. Microbiol. **36**(1-2), 47–54 (2003).
29. X.-Y. Zhang, Y.-S. Yu, C.-C. Zhu, C. Chen, R. Yang, Y. Xue, Q.-D. Chen, and H.-B. Sun, "Miniature end-capped fiber sensor for refractive index and temperature measurement," IEEE Photonics Technol. Lett. **26**(1), 7–10 (2014).
30. V. A. Márquez-Cruz and J. A. Hernández-Cordero, "Fiber optic Fabry-Perot sensor for surface tension analysis," Opt. Express **22**(3), 3028–3038 (2014).
31. T. Kohl and C. Ascoli, "Protocol: Indirect Immunometric ELISA," Cold Spring Harb Protoc. **125**, 1128–1129 (2003).
32. S. Liu, Z. Deng, J. Li, J. Wang, N. Huang, R. Cui, Q. Zhang, J. Mei, W. Zhou, C. Zhang, Q. Ye, and J. Tian, "Measurement of the refractive index of whole blood and its components for a continuous spectral region," J. Biomed. Opt. **24**(3), 1–5 (2019).
33. H. Li, L. Lin, and S. Xie, "Refractive index of human whole blood with different types in the visible and near-infrared ranges," in *Laser-Tissue Interaction XI: Photochemical, Photothermal, and Photomechanical*, vol. 3914 (International Society for Optics and Photonics, 2000), pp. 517–521.
34. R. Bruck, E. Melnik, P. Muellner, R. Hainberger, and M. Lämmerhofer, "Integrated polymer-based Mach-Zehnder interferometer label-free streptavidin biosensor compatible with injection molding," Biosens. Bioelectron. **26**(9), 3832–3837 (2011).
35. B. E. Schubert and D. Floreano, "Variable stiffness material based on rigid low-melting-point-alloy microstructures embedded in soft poly (dimethylsiloxane) (PDMS)," RSC Adv. **3**(46), 24671–24679 (2013).
36. B.-B. Li, Q.-Y. Wang, Y.-F. Xiao, X.-F. Jiang, Y. Li, L. Xiao, and Q. Gong, "On chip, high-sensitivity thermal sensor based on high-q polydimethylsiloxane-coated microresonator," Appl. Phys. Lett. **96**(25), 251109 (2010).
37. D. C. Company, "Sylgard 184 silicone elastomer," (2017).
38. K. Wysokiński, D. Budnicki, J. Fidelus, Ł. Szostkiewicz, Ł. Ostrowski, M. Murawski, M. Staniszewski, M. Staniszewska, M. Napierała, and T. Nasiłowski, "Dual-core all-fiber integrated immunosensor for detection of protein antigens," Biosens. Bioelectron. **114**, 22–29 (2018).